PROTEINS: Structure, Function, and Bioinformatics 60:401–411 (2005)

Increasing the Molecular Contacts Between Maurotoxin and Kv1.2 Channel Augments Ligand Affinity

Sarrah M'Barek,[1] Benjamin Chagot,[2] Nicolas Andreotti,[1,3] Violeta Visan,[4] Pascal Mansuelle,[1] Stephan Grissmer,[4] Mohamed Marrakchi,[5] Mohamed El Ayeb,[6] François Sampieri,[1] Hervé Darbon,[2] Ziad Fajloun,[3] Michel De Waard,[7] and Jean-Marc Sabatier[1,3]*

[1]*Laboratoire d'Ingénierie des Protéines, CNRS FRE 2738, IFR Jean Roche, Faculté de Médecine Nord, Marseille, France*
[2]*Architecture et Fonction des Macromolécules Biologiques, CNRS UMR 6098, Marseille, France*
[3]*Laboratoire Cellpep, Marseille, France*
[4]*Universität Ulm, Ulm, Germany*
[5]*Génétique Moléculaire, Immunologie et Biotechnologie, Faculté des Sciences de Tunis, Tunis, Tunisia*
[6]*Laboratoire des Venins et Toxines, Institut Pasteur de Tunis, Tunis, Tunisia.*
[7]*Laboratoire Canaux Calciques, Fonctions et Pathologies, Inserm U607, CEA, DRDC, Grenoble, France*

ABSTRACT **Scorpion toxins interact with their target ion channels through multiple molecular contacts. Because a "gain of function" approach has never been described to evaluate the importance of the molecular contacts in defining toxin affinity, we experimentally examined whether increasing the molecular contacts between a toxin and an ion channel directly impacts toxin affinity. For this purpose, we focused on two scorpion peptides, the well-characterized maurotoxin with its variant Pi1-like disulfide bridging (MTX_{Pi1}), used as a molecular template, and butantoxin (BuTX), used as an N-terminal domain provider. BuTX is found to be 60-fold less potent than MTX_{Pi1} in blocking Kv1.2 (IC_{50} values of 165 nM for BuTX versus 2.8 nM for MTX_{Pi1}). Removal of its N-terminal domain (nine residues) further decreases BuTX affinity for Kv1.2 by 5.6-fold, which is in agreement with docking simulation data showing the importance of this domain in BuTX-Kv1.2 interaction. Transfer of the BuTX N-terminal domain to MTX_{Pi1} results in a chimera with five disulfide bridges (BuTX-MTX_{Pi1}) that exhibits 22-fold greater affinity for Kv1.2 than MTX_{Pi1} itself, in spite of the lower affinity of BuTX as compared to MTX_{Pi1}. Docking experiments performed with the 3-D structure of BuTX-MTX_{Pi1} in solution, as solved by ^{1}H-NMR, reveal that the N-terminal domain of BuTX participates in the increased affinity for Kv1.2 through additional molecular contacts. Altogether, the data indicate that acting on molecular contacts between a toxin and a channel is an efficient strategy to modulate toxin affinity. Proteins 2005;60:401–411.** © 2005 Wiley-Liss, Inc.

Key words: maurotoxin; butantoxin; scorpion toxin; chimera toxin; K^+ channels; molecular contacts; toxin affinity

INTRODUCTION

Maurotoxin (MTX) is a short-chain 34-mer toxin, cross-linked by four disulfide bridges, that has been isolated initially from the venom of the scorpion *S. maurus palmatus*.[1] MTX is reportedly active on voltage-gated Kv1.2 channels at low nanomolar concentrations.[2,3] Additionally, it blocks small (SKCa) and intermediate (IKCa) Ca^{2+}-activated K^+ channels.[4] MTX has been used extensively in structure-activity studies, such as those investigating the role of disulfide bridges in toxin folding[2,5–8] or the contribution of the α-helical and β-sheet regions in toxin pharmacology.[9] Recently, we have also used MTX as a template to produce a chimera molecule with *H. spinnifer* toxin 1 (HsTx1). The latter possesses the high affinity of MTX for SKCa channels and the high affinity of HsTx1 for Kv1.1 and Kv1.3 channels.[9] This example demonstrates that swapping of toxin domains can be a successful approach to produce new analogs with interesting pharmacological characteristics. In this manuscript, we extended on this observation by focusing on the contribution of the

Abbreviations used: BuTX, Butantoxin (toxin from the Brazilian scorpion *Tityus serrulatus*); $BuTX_{\Delta 1-9}$, Butantoxin analogue with a truncated N-terminal extremity (deletion of BuTX region 1–9); BuTX-MTX_{Pi1}, chimera between BuTX (nine N-terminal residues; region 1–9 of BuTX) and MTX_{Pi1} (last thirty two residues; region 3–34 of MTX); CNS, crystallography and NMR system (a software suite for macromolecular structure determination); DMSO, Dimethylsulfoxide; HPLC, High pressure liquid chromatography; HsTx1, Toxin 1 from the scorpion *Heterometrus spinnifer*; IC_{50}, 50% inhibitory concentration; IKCa1 channel, Intermediate-conductance Ca^{2+}-activated K^+ channel; Kv channel, Mammalian voltage-gated K^+ channel; MALDI-TOF, Matrix-assisted laser desorption ionization-time-of-flight; MTX, maurotoxin (toxin from the scorpion *S. maurus palmatus*); MTX_{Pi1}, MTX with a Pi1-like disulfide bridge organization of the type C1–C5, C2–C6, C3–C7 and C4–C8; NOE, Nuclear Overhauser Effect; NOESY, NOE spectroscopy; NMP, N-methylpyrrolidone; Pi1, Pi4 and Pi7, Toxins 1, 4 and 7 from the scorpion *Pandinus imperator*; SK channel (or SKCa channel), Small-conductance Ca^{2+}-activated K^+ channel; TFA, Trifluoroacetic acid; TOCSY, Total correlation spectroscopy; $\Delta\epsilon E$, Energy derivative during minimization.

*Correspondence to: Jean-Marc Sabatier, Laboratoire d'Ingénierie des Protéines, CNRS FRE 2738, IFR Jean Roche, Faculté de Médecine Nord, Bd Pierre Dramard, 13916, Marseille Cedex 20, France. E-mail: sabatier.jm@jean-roche.univ-mrs.fr

Received 25 November 2004; Revised 19 January 2005; Accepted 2 February 2005

Published online 21 June 2005 in Wiley InterScience (www.interscience.wiley.com). DOI: 10.1002/prot.20509

number of molecular contacts in toxin affinity. In particular, we wanted to use this toxin domain swapping strategy in a "gain of function" approach by which we would increase the affinity of the template toxin for its target channel. For this purpose, we found relevant to choose MTX as a template and Kv1.2 as the target channel since the affinity of MTX for Kv1.2 is already high. We thus aimed at removing a limited nonrelevant N-terminal domain of MTX to replace it by another N-terminal domain from a distinct toxin—also active on Kv1.2—predicted to make molecular contacts with Kv1.2. Although we did not dispose of complementary toxin/channel mutagenesis data to define the toxin domains to be transferred, we based our strategy on docking simulation experiments. As domain donor for sequence swapping, we chose butantoxin (BuTX), a 40-mer toxin from the Brazilian scorpion *Tityus serrulatus*.[10,11] This toxin was shown to block reversibly the voltage-gated K^+ channels (*Shaker* B and Kv1.2). The resulting chimera encompasses residues 1 to 9 of BuTX at its N-terminus, and residues 3 to 34 of MTX at its C-terminus. The molecule was chemically synthesized by an optimized Fmoc/t-butyl strategy,[12] and its disulfide bridge organization was formally determined by enzyme cleavage of the folded/oxidized product. The pharmacology of the chimera was also functionally evaluated in vitro in comparison with those of parent molecules and an N-terminal truncated form of BuTX. Because the chimera was found to be more potent in blocking Kv1.2 currents than the parent toxins, its 3-D structure in solution was determined by ^{1}H-NMR, and used in docking simulation experiments onto a molecular model of the Kv1.2 ion channel pore. The data demonstrate that the additional molecular contacts, introduced by inserting the N-terminal domain of BuTX into the chimera molecule, are responsible for an increased affinity of the chimera toward the Kv1.2 channel.

EXPERIMENTAL PROCEDURES

Materials

N-α-Fluoren-9-ylmethyloxycarbonyl (Fmoc)-L-amino acids, Fmoc-amide resin, and reagents used for chemical peptide syntheses were purchased from Perkin-Elmer. Solvents were analytical grade products from SDS (Peypin, France). Trypsin and chymotrypsin were purchased from Sigma. The tsA cell line expressing human IKCa1 channel was a kind gift from Dr. Devor (University of Pittsburg, PA). The mammalian B82 mouse fibroblast cell line stably expressing rat Kv1.2 was described previously.[12]

Chemical Peptide Synthesis

The peptides (BuTX, $BuTX_{\Delta 1-9}$, MTX_{Pi1}, and BuTX-MTX_{Pi1}) were chemically produced by the solid-phase method[13] using an automated peptide synthesizer (Model 433A, Applied Biosystems, Inc.). The synthesis of MTX_{Pi1} was described previously.[6] Other peptide chains were assembled by stepwise synthesis on 0.3 mmol of Fmoc-amide resin (1% cross-linked; 0.65 mmol of amino group/g) using 1 mmol of Fmoc-amino acid derivatives. The side-chain protecting groups of trifunctional residues were: *tert*-butyl for Ser, Thr, Tyr, Glu, and Asp; trityl (Trt) for Cys, Asn, and Gln; pentamethylchroman for Arg, and *tert*-butyloxycarbonyl for Lys and Trp. *N*-α-amino groups were deprotected by treatments with 18% and 20% (v/v) piperidine/*N*-methylpyrrolidone (NMP) for 3 and 8 min, respectively. The peptide-resins were washed with NMP (5 × 1 min), and then Fmoc-amino acid derivatives were coupled (20 min) as their hydroxybenzotriazole active esters in NMP (3.3-fold excess). After each peptide chain assembly was completed and the N-terminal Fmoc group removed, peptide-resins (2.1–2.8 g) were treated, under stirring, for 3 h at room temperature, with a mixture of trifluoroacetic acid/H_2O/thioanisole/ethanedithiol (88:5:5:2, v/v) in the presence of crystalline phenol (2.5 g), in a final volume of 30 ml per gram of peptide-resin. The peptide mixtures were filtered to remove the resin, and the filtrates were precipitated and washed twice in cold diethylether. The crude peptides were then pelleted by centrifugation (3,000g; 10 min) and the supernatants were discarded. The peptides were finally dissolved in H_2O, freeze dried and lyophilized. The crude peptides were then dissolved in 0.2 M Tris-HCl buffer, pH 8.4 (with 10% (v/v) dimethylsulfoxide (DMSO) in the case of BuTX and BuTX-MTX_{Pi1}), to a final peptide concentration of ca. 2 mM, then gently stirred under air to allow oxidative folding (72 h, 25°C). The peptides were purified to homogeneity (> 98%) by semi-preparative reversed-phase high-pressure liquid chromatography (HPLC) (Perkin-Elmer, C_{18} Aquapore ODS 20 μm, 250 × 10 mm), by means of a 60 min linear gradient from 0% to 35% of buffer B (0.08% (v/v) TFA/acetonitrile) in buffer A (0.1% (v/v) TFA/H_2O), at a flow rate of 6 ml/min (λ = 230 nm). The identity and degree of homogeneity of the peptides were verified by: (1) analytical C_{18} reversed-phase HPLC (Chromolith RP18, 5 μm, 4.6 × 100 mm) using a 40-min linear gradient from 0% to 60% of buffer B (0.08% (v/v) TFA/acetonitrile) in buffer A (0.1% (v/v) TFA/H_2O), at a flow rate of 1 ml/min; (2) amino acid analysis after acidolysis (6 N HCl/2% (w/v) phenol, 20 h, 118°C, N_2 atmosphere); (3) Edman sequencing; and (4) molecular mass analysis by matrix-assisted laser desorption ionization-time of flight (MALDI-TOF) mass spectrometry.

Assignment of Half-Cystine Pairings of Peptides

The peptides (600 μg) were each added to a mixture of 10% (w/w) of trypsin and chymotrypsin, in 0.2 M Tris-HCl buffer (pH 7.4) (14 h, 37°C). The resulting peptide fragments were then separated by analytical reversed-phase HPLC (Chromolith RP18, 5 μm, 4.6 × 100 mm) in a 60-min linear gradient from 0% to 60% of buffer B (0.08% (v/v) TFA/acetonitrile) in buffer A (0.1% (v/v) TFA/H_2O), at a flow rate of 1 ml/min (λ = 230 nm), and freeze-dried prior to their analyses. The peptides were hydrolyzed (6 N HCl/phenol, 110°C) and their amino acid contents determined (Beckman, System 6300 amino acid analyzer). The peptides were also analyzed by mass spectrometry (RP-DE

Voyager, Perseptive Biosystems), and Edman sequencing using a gas-phase microsequencer (Applied Biosystems 470A). In standard HPLC conditions for analyzing phenylthiohydantoin (PTH) amino acid derivatives, the diPTH-cystine eluted at a retention time of 9.8 min.

Electrophysiology

All the experiments were carried out at room temperature (22–25°C) using the whole-cell recording mode of the patch-clamp technique.[14,15] Cells were bathed with an extracellular Ringer's solution containing (in mM): 160 NaCl, 4.5 KCl, 2 $CaCl_2$, 1 $MgCl_2$, and 10 HEPES (pH 7.4) (with NaOH), with an osmolarity of 290–320 mOsm. To prevent nonspecific binding of toxin to the recording chamber, 0.1% bovine serum albumin was added to the Ringer's solution. For measuring Kv1.2 currents, the internal pipette solution contained (in mM): 155 KF, 2 $MgCl_2$, 10 HEPES, and 10 EGTA, pH 7.2 (with KOH), with an osmolarity of 290–320 mOsm. For measuring IKCa1 currents, we used an internal pipette solution containing (in mM): 135 K-aspartate, 8.7 $CaCl_2$, 2 $MgCl_2$, 10 EGTA, 10 HEPES (pH 7.2) (with KOH), with an osmolarity of 290–320 mOsm, (free $[Ca^{2+}]_i = 10^{-6}$ M). Electrodes had resistances of 2.5–5 MΩ. Membrane currents were measured with an EPC-9 patch-clamp amplifier (HEKA Elektronik, Lambrecht, Germany) interfaced to a Macintosh computer running acquisition and analysis software (Pulse and PulseFit). Capacitive and leak currents were subtracted using the P/10 procedure. Series resistance compensation (> 80%) was employed if the current exceeded 2 nA. The holding potential in all experiments was −80 mV. Data analysis was performed in IgorPro, and K_d values were deduced by fitting a modified Hill equation ($I_{toxin}/I_{control} = 1/[1 + ([toxin]/K_d)]$), with a Hill coefficient of 1, to normalized data points. The value of each peptide concentration was the mean of at least three measurements.

Circular Dichroism Analysis of BuTX-MTX_{Pi1}

The circular dichroism (CD) spectrum was obtained on a Jasco J-810 spectropolarimeter equipped with a PTC-423S thermostat. A ratio of 2.20 was found between the positive CD band at 290.5 nm and the negative band at 192.5 nm. The CD spectrum was reported as the absorption coefficient ($\Delta\epsilon$) per amide. The far UV CD spectrum was acquired at 20°C in H_2O between 185 and 260 nm using 0.1-cm path length cell. Data were collected twice at 0.6 nm intervals with a scan rate of 50 nm/min. As assessed by amino acid analysis, the concentration of BuTX-MTX_{Pi1} was 40 nM.

Three-Dimensional Structure of BuTX-MTX_{Pi1} in Solution as Determined by ^{1}H-NMR

NMR experiments

The ^{1}H-NMR spectra were all recorded on a BRUKER DRX500 spectrometer equipped with an HCN probe and self shielded triple axis gradients were used. The experiments were performed at two temperatures (290 and 310 K) in order to solve assignment uncertainties. Two-dimensional spectra were acquired using the States-TPPI method to achieve F1 quadrature detection.[16,17] Water suppression was obtained either using presaturation during the 1.3 sec relaxation delay and during the mixing time for NOESY spectra, or with a watergate 3-9-19 pulse train using a gradient at the magic angle obtained by applying simultaneous x-, y- and z- gradients prior to detection.[18] TOCSY were performed with a spin-lock time of 80 msec and a spin locking field strength of 8 kHz. The mixing time of the NOESY experiments was set to 80 msec. The individual amide proton exchange rates were determined by recording one series of four NOESY spectra (each experiment was 10 h long) at 280 K on the D_2O sample. Amide protons still giving rise to Nuclear Overhauser Effect (NOE) correlations after 40 h of exchange were considered as slowly exchanging and therefore engaged in a hydrogen bond.

Analysis of spectra

The identification of amino acid spin systems and the sequential assignment were achieved using the two-step standard strategy described by Wüthrich and applied with the XEASY graphical software.[19,20] The comparative analysis of COSY and TOCSY spectra recorded in water gave the spin system signatures of the BuTX-MTX_{Pi1}. The spin systems were then sequentially connected using the NOESY spectra.

Experimental restraints

The integration of NOE data was performed by measuring the peak volumes and by using a routine of XEASY. The Φ torsion angle constraints resulted from the $^3J_{HN\text{-}H\alpha}$ coupling constant measurements that were measured on a COSY spectrum with 8192 data points in the acquisition dimension. These Φ angles were restrained to $-120 \pm 40°$ for a $^3J_{HN\text{-}H\alpha} > 8$ Hz and to $-65 \pm 25°$ for a $^3J_{HN\text{-}H\alpha} \leq 6$ Hz. No angle constraint was assigned to a $^3J_{HN\text{-}H\alpha} = 7$ Hz, a value considered as ambiguous.

Determination of the amide proton exchange rates led us to identify protons involved in hydrogen bonding. The oxygen partners were then identified by visual inspection of the preliminary calculated structures.

Structure calculation

The distance restraints (from measured NOE volumes), dihedral angles (from $^3J_{HN\text{-}H\alpha}$ coupling constants), restraints from disulfides bridges and from hydrogen bonds were used in structural calculations to determine toxin conformation. These restraints were introduced as input in ARIA implemented in CNS 1.1.[21,23] In the first run, the calculation was initiated using NOESY pick list, dihedral angles restraints and the assignment of experimentally determined disulfide bridges. This first run allowed us to correct NOE assignment and gave rise to a preliminary fold that was used to detect hydrogen bonds carbonyl partners. In the second run, distance restraints, dihedral angles, hydrogen bonds and disulfide bridges were used. We calculated 100 structures in the final iteration and 50

structures were kept for minimization in water. The 25 best structures were finally kept as defining the conformation of BuTX-MTX_{Pi1} chimera. Visual analysis of the final selected structures was carried out with the TURBO graphic software and the geometric quality of the resulting structures was assessed with the PROCHECK 3.4 and PROCHECK-NMR softwares.[23,24] The 3-D structure of BuTX-MTX_{Pi1} is deposited at the PDB (code 1WT7). The assigned chemical shifts of the chimera are deposited at the BioMagResBank (BMRB accession number 6389).

Docking of BuTX, MTX_{Pi1} and BuTX-MTX_{Pi1} onto Kv1.2 Channel

Molecular modeling

Atomic coordinates of BuTX (Swiss-Prot # 1C55)[10] was obtained from the Swiss Protein Database (www.expasy.ch). The computed molecular model of MTX_{Pi1} was generated as previously described.[6] Molecular modelling of the S5-H5-S6 pore region of Kv1.2 channel was achieved on the basis of the crystal structure of KvAP, a voltage-dependent K^+ channel from *Aeropyrum pernix*, solved at 3.2 Å (Swiss-Prot # 1ORQ).[25] The 3D model of this region was generated using the Biopolymer Homology modelling software of Swiss-model/Deep view 3.7 (Swiss-Prot, Switzerland). The sequence alignment of KvAP with Kv1.2, generated with CLUSTALW (v.1.82 www.ebi.ac.uk/clustalw/), shows sequence homology of 68.9%. To avoid steric overlaps and clashes, modelled side-chains and channel Cα trace were subjected to energy refinement (until $\Delta\epsilon E < 0.05$ kJ.mol^{-1}.Å^{-1}) using steepest-descent, conjugate gradient and Newton Raphson algorithms successively, with the CVFF force-field as implemented in the INSIGHT II discover3 module (1998 release, Molecular Simulations Inc., ACCELRYS, San Diego CA). RMSD values between the Cα KvAP template and the Cα Kv1.2 model is 0.21 Å. Side-chain RMSD variations of Kv1.2 after minimization was 0.82 Å, when compared with the unrefined model. The four Kv1.2 channel subunits were labelled as I–IV.

Protein docking

Molecular interaction simulations were performed using the BiGGER program (bimolecular complex generation with global evaluation and ranking).[26] In a first step, a 1-Å 3D matrix composed of small cubic cells, which represents the complex shape of each molecule, was generated. The translational interaction space was searched for each relative orientation of the two molecules by systematically shifting the probe matrix (toxin) to the target matrix (ion channel). Five thousand docking solutions were selected after the probe rotation by 15° increments, relative to the target, and this surface matching was repeated until a complete nonredundant search was achieved. The algorithm used by BiGGER performs a complete and systematic search for surface complementarities (both geometry complementarities and amino acid residue pairwise affinities are considered) between two potentially interacting molecules, and enables an implicit treatment of molecular flexibility. In the second step, the 5,000 putative solutions were ranked according to four different interaction terms: surface matching, side chain contacts, electrostatic and solvation energies combined into a global scoring function. The 15 best docking solutions were selected according to (1) the global score computed by BiGGER, (2) the functional dyad,[27] (3) the β-sheet structure orientation toward the Kv1.2 channel pore, and (4) the global orientation relative to the electrostatic properties of both toxins/chimera and channel. The GRASP software was used to determine such electrostatic properties (GRASP, Howard Hughes Medical Institute, Colombia University, NY).[28]

Structural refinement of final complexes

The screened docking solutions were energy-minimized according to a rigid-body method (Cα–Cα distances locked) with the steepest-descent algorithms, using Deep-view V3.7 (until $\Delta\epsilon E < 0.05$ kJ.mol^{-1}.Å^{-1}) with a GROMOS96 force-field to relieve possible steric clashes and overlaps.[29] During structural refinement, a distance-dependent dielectric constant of 4 was used. Final docking energy of each best solution was obtained according to the formula: Docking energy = $\epsilon_{toxin\text{-}channel} - (\epsilon_{toxin} + \epsilon_{channel})$, where ϵ_{toxin} represents the toxin energy alone, $\epsilon_{channel}$ the channel energy alone, both energies being determined after rigid body minimization until $\Delta\epsilon E < 0.05$ kJ.mol^{-1}.Å^{-1} (Cα–Cα distances locked, GROMOS96 force field),[29] and $\epsilon_{toxin\text{-}channel}$ the final complex energy minimized under identical conditions until $\Delta\epsilon E < 0.05$ kJ.mol^{-1}.Å^{-1} (Cα locked, GROMOS96 force field). Details of interactions were analyzed using the LIGPLOT program on each best docking solution provided by the screening method.[30] Linear regression was computed using SigmaPlot 8.02 (RockWare Inc.).

RESULTS AND DISCUSSION

Design of the Chimera

In previous studies,[5,31,32] in which we altered MTX structure, we generally shifted the disulfide bridge organization of MTX from a C1-C5, C2-C6, C3-C4 and C7-C8 pattern (nonconventional) to a C1-C5, C2-C6, C3-C7, and C4-C8 pattern (conventional). The conventional pattern is also found in Pi1, Pi4, Pi7, and HsTx1, four toxins belonging to the same α-KTx6 family.[33] This MTX variant, termed MTX_{Pi1}, has been characterized from a structural and functional point of view.[6] For Kv1.2, the MTX variant has a 46-fold reduction in affinity as compared to MTX.[6] In the following sections, we will refer to MTX_{Pi1} instead of MTX since, as expected, the MTX part of the BuTX-MTX chimera adopts the conventional MTX_{Pi1} disulfide bridging (see Results section). Accordingly, pharmacological properties of the BuTX-MTX_{Pi1} chimera are compared to those of MTX_{Pi1}. The amino acid sequences and disulfide bridge patterns of MTX_{Pi1} and BuTX are shown for comparison in Figure 1(a). BuTX belongs to the α-KTx12 family and displays half-cystine pairings of the C1-C2, C3-C6, C4-C7, and C5-C8 type.[33] An amino acid sequence alignment between MTX_{Pi1} and BuTX illustrates that

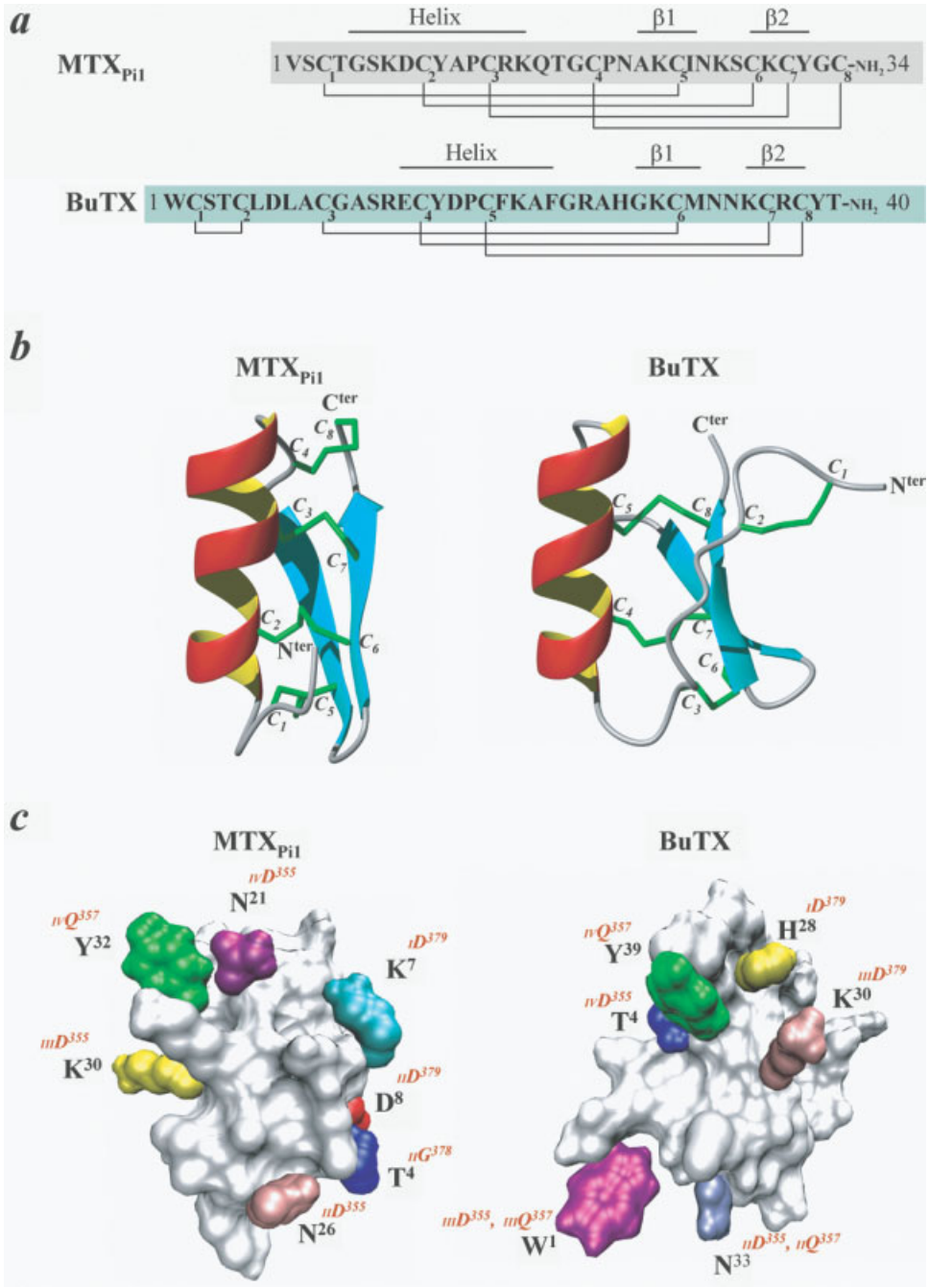

Fig. 1. Structural comparison between MTX_{Pi1} and BuTX, and docking simulations on the Kv1.2 channel pore. **a:** amino acid sequences (*one-letter-code*) and half-cystine pairings of MTX_{Pi1} and BuTX. Half-cystine residues are numbered by order of appearance from the N- to the C-terminus. The relative positioning of secondary structures (helix and β strands of the β-sheet structure) is indicated for each peptide. Disulfide bridges are depicted by plain lines. **b:** Molecular model of MTX_{Pi1} and ^{1}H-NMR 3-D solution structure of BuTX. The helix, β-sheet and disulfide bridges are highlighted in red, blue and green, respectively. Half-cystine residues are numbered as in parts (a) and (**c**), Theoretical functional maps of MTX_{Pi1} and BuTX highlighting amino acid residues that are key for peptide interaction with Kv1.2 channel (colored residues). Interacting residues from the Kv1.2 channel are shown in red. I to IV before channel residue numbering specifies one of the four α-subunits forming the functional Kv1.2 channel. These maps were generated by docking simulations.

BuTX possesses an extended N-terminal domain, not present in MTX_{Pi1}. However, both peptides fold according to the classical α/β scaffold, an architectural motif composed of an helical structure connected to a β-sheet (two or three strands) by two disulfide bridges.[10,27,34,35] Of note, although MTX_{Pi1} and BuTX are both cross-linked by four disulfide bridges, the positioning and arrangement of these disulfide bridges are partially conserved. This is highlighted in a structural comparison between MTX_{Pi1} and BuTX [Fig. 1(b)]. In particular, the C1-C5, C2-C6 and C3-C7 half-cystine pairs of MTX_{Pi1} play structural roles similar to the C3-C6, C4-C7 and C5-C8 pairs of BuTX. The last C4-C8 connection in MTX_{Pi1}, that reduces the mobility of the C-terminal domain of MTX_{Pi1}, does not exist in BuTX. Conversely, the C1-C2 connection of BuTX is lacking in MTX_{Pi1} and thus defines an additional extended N-terminal domain. This structural comparison provides a first rationale for domain swapping in the design of chimeras indicating that the N-termini of both toxins might be appropriate candidates for such a swapping (two first MTX_{Pi1}residues, and nine first BuTX residues). Next, we examined by docking simulation experiments whether these two domains possess the ideal characteristics: that is, no interaction of the two first residues of MTX_{Pi1} with Kv1.2 (VS motif), and some molecular contacts within the N-terminal part of BuTX [Fig. 1(c)]. According to docking simulations, MTX_{Pi1} is found to interact with Kv1.2 through seven main molecular contacts, whereas the interaction of BuTX requires six main contacts. The few contacts of BuTX docking onto Kv1.2 channel may explain its weak activity. However, it appears that this toxin could be stabilized over the pore of the channel by several electrostatic interactions between the N-terminal region of the toxin and the turret region. Of interest, Trp^1 and Thr^4 of BuTX are also found to interact with residues $IIIGln^{357}$/$IIIAsp^{355}$ and $IVAsp^{355}$ of Kv1.2, respectively. In contrast, Val^1 and Ser^2 of MTX_{Pi1} are not involved in any kind of interaction with Kv1.2. Altogether, these observations suggest that swapping the first two amino acid residues of MTX_{Pi1}, by the nine N-terminal residues of BuTX, would constitute an interesting molecular basis to investigate whether the addition of novel molecular contacts within MTX_{Pi1} is beneficial for Kv1.2 current blockage efficacy. Before investigating the properties of such a chimera, we first confirmed experimentally that the N-terminal domain of BuTX participates in defining the affinity of BuTX for Kv1.2 channel. A truncated form of BuTX ($BuTX_{Δ1-9}$) was chemically produced [Fig. 2(a,b)]. HPLC profiles of the product at different stages of its chemical synthesis are illustrated in Figure 2(a). The purified $BuTX_{Δ1-9}$ possesses an experimental *M*r $(M+H)^+$ of 3520.7, consistent with its theoretical *M*r $(M+H)^+$ of 3521.1. Half-cystine pairs of synthetic $BuTX_{Δ1-9}$ were determined by enzyme cleavage followed by analysis of the resulting peptide fragments (data not shown). The disulfide bridges were thereby mapped between Cys^{10}-Cys^{31}, Cys^{16}-Cys^{36}, and Cys^{20}-Cys^{38}, a pattern of connection similar to that found in BuTX itself. We also chemically produced BuTX and

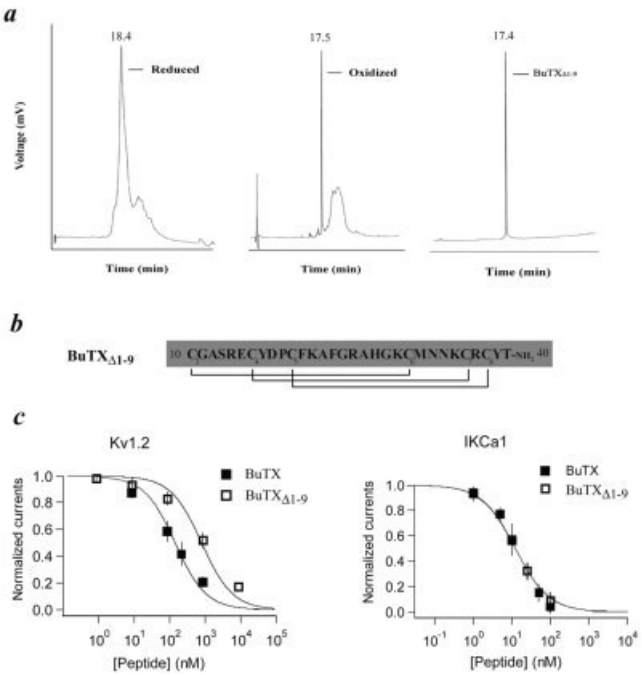

Fig. 2. $BuTX_{Δ1-9}$: chemical synthesis, disulfide bridge organization and pharmacology. **a:** $BuTX_{Δ1-9}$ at different stages of its chemical synthesis. HPLC profiles of the crude reduced peptide (left), crude peptide after oxidative folding (middle), and purified $BuTX_{Δ1-9}$ (right). **b:** Amino acid sequence (*one-letter-code*) and half-cystine pairings of the N-terminal truncated 31-mer analog of BuTX ($BuTX_{Δ1-9}$). Assignment of the half-cystine pairings was achieved by analysis of the peptides yielded by enzyme cleavage (trypsin and chymotrypsin) of $BuTX_{Δ1-9}$ (data not shown). Half-cystine residues are numbered according to their regular positions in the BuTX sequence. **c:** Concentration-dependent inhibition curves of Kv1.2 (left) and IKCa1 (right) currents by BuTX (■) and $BuTX_{Δ1-9}$ (□). Fits of the data yield IC_{50} values of 165 ± 20 nM (BuTX) and 919 ± 287 nM ($BuTX_{Δ1-9}$) for Kv1.2 and of 12.3 ± 1.3 nM (BuTX) and 12.5 ± 0.9 nM ($BuTX_{Δ1-9}$) for IKCa1.

checked that the synthetic product conformed to the description of native BuTX, notably a disulfide bridge arrangement of the type C1-C2, C3-C6, C4-C7 and C5-C8;[10] (data not shown). We next evaluated and compared the ability of $BuTX_{Δ1-9}$ and BuTX to block Kv1.2 potassium currents [Fig. 2(c, left)]. Here, the activity of BuTX on Kv1.2 is described for the first time. The toxin blocks the current with an IC_{50} value of 165 ± 21 nM. In comparison, $BuTX_{Δ1-9}$ is 5.6-fold less active, with an IC_{50} value of 919 ± 287 nM. These data suggest that the nine-residue N-terminal domain of BuTX participates in the affinity of BuTX for the Kv1.2 channel. This is coherent with our docking simulations showing that two residues (Trp^1 and Thr^4) from the BuTX N-terminal domain are in close contacts with residues of the pore region of Kv1.2 [Fig. 1(c)]. In a recent work, we evidenced that the β-sheet structure of some related scorpion toxins behaves as the main determinant for recognition and blocking of IKCa1 channel.[4,9] We first evaluated whether BuTX could act on IKCa1 channel [Fig. 2(c, right)]. BuTX was found to block IKCa1 currents, with an IC_{50} value of 12.3 ± 1.3 nM. Interestingly, $BuTX_{Δ1-9}$ acts on this channel with a

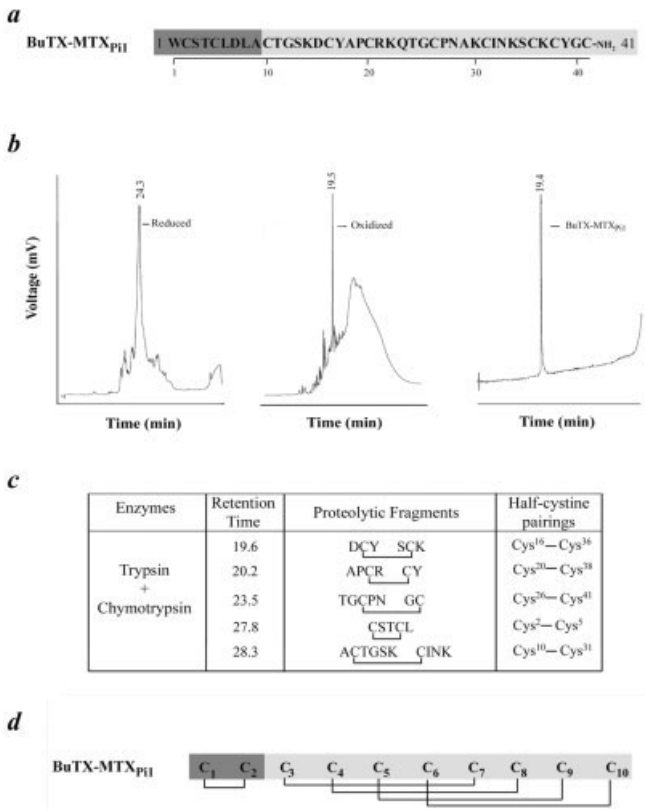

Fig. 3. BuTX-MTX$_{Pi1}$: chemical synthesis and disulfide bridge pattern. **a:** Amino acid sequence of the 41-mer BuTX-MTX$_{Pi1}$ chimera. Amino acid sequences derived from BuTX and MTX are shaded in dark and light grey, respectively. **b:** BuTX-MTX$_{Pi1}$ at different stages of its chemical synthesis. HPLC profiles of the crude reduced peptide (left), crude peptide after oxidative folding (middle), and purified BuTX-MTX$_{Pi1}$ (right). **c:** Assignment of the half-cystine pairings by analysis of the peptide fragments yielded by enzyme cleavage (trypsin and chymotrypsin) of BuTX-MTX$_{Pi1}$. **d:** Disulfide bridge pattern of BuTX-MTX$_{Pi1}$.

similar IC_{50} value of 12.5 ± 0.9 nM. This observation indicates that the N-terminal domain of BuTX does not contribute to the toxin activity on IKCa1. Therefore, the N-terminal domain of BuTX may be tentatively used as a donor domain to design an MTX-derived molecule with an increased affinity for Kv1.2.

Production of the BuTX-MTX$_{Pi1}$ Chimera

The designed chimera encompasses the N-terminal domain of BuTX (residues 1–9), the rest of the molecule being derived from the MTX amino acid sequence [residues 3–34, Fig. 3(a)]. BuTX-MTX$_{Pi1}$ was synthesized using an optimized Fmoc/t-butyl strategy.[12] HPLC profiles of elution are shown at different stages of chimera synthesis [Fig. 3(b)]. Mass spectrometry analysis of BuTX-MTX$_{Pi1}$ gave an experimental *M*r $(M+H)^+$ of 4417.7, consistent with its deduced *M*r $(M+H)^+$ of 4417.8. Amino acid analysis of BuTX-MTX$_{Pi1}$ after acidolysis provides an amino acid content that fully agrees with the deduced values (data not shown). To determine the pattern of half-cystine pairings, BuTX-MTX$_{Pi1}$ was cleaved by a mixture of trypsin and chymotrypsin. The resulting peptide fragments were purified to homogeneity by HPLC, and characterized by means of amino acid analysis, mass spectrometry, and Edman sequencing techniques [Fig. 3(c)]. The half-cystine pairings are thereby mapped as Cys^2-Cys^5, Cys^{10}-Cys^{31}, Cys^{16}-Cys^{36}, Cys^{20}-Cys^{38}, and Cys^{26}-Cys^{41} [Fig. 3(d)]. Thus, the chimera is cross-linked by five disulfide bridges, the first one being borrowed from BuTX and the remaining four from MTX in its Pi1-like disulfide bridge arrangement. These data confirm earlier observations indicating that alteration of the MTX structure favors a disulfide bridge rearrangement from the nonconventional to the conventional pattern.[5,32]

Three-dimensional Solution Structure of the BuTX-MTX$_{Pi1}$ Chimera

Since the chimera is highly reticulated with five disulfide bridges for 41 amino acid residues (ca. 25% of half-cystine residues in the peptide composition), we first assessed its structural features using a preliminary circular dichroism analysis [Fig. 4(a)]. Measurements were performed at a wavelength ranging from 185–260 nm. The data obtained correspond essentially to π-π* and n-π* transitions of the amide chromophores of the peptide backbone.[36] The CD spectrum showed a large negative contribution between 200 and 235 nm, and a large positive contribution around 190 nm, indicating the presence of both helical and β-sheet secondary structures. These data are coherent with a folding of the chimera according to a α/β scaffold.[27,34,37] Next, we pursued with solving the 3-D structure of BuTX-MTX$_{Pi1}$ in solution by ^{1}H-NMR. For NMR resonance assignment and secondary structures, the spin systems were identified on the basis of both COSY and TOCSY spectra. Once the sequential assignment was achieved, almost all protons were identified and their resonance frequencies determined. The distribution of the $H\alpha_i/HN_{i+1}$, HN_i/HN_{i+1} and $H\alpha_i/HN_{i+3}$ correlation, the coupling constants and amide proton exchange rates are presented in [Fig. 4(b)]. The HN_i/HN_{i+1} correlation, associated with hydrogen bonds and small coupling constants, in the Ser^{13}-Gln^{23} stretch are characteristic of a helical region. Strong $H\alpha/HN_{i+1}$ correlation, associated with large coupling constants, from Asn^{28} to Cys^{38}, are characteristic of an extended region. The structure of BuTX-MTX$_{Pi1}$ was solved by using 482 NOE-based distance restraints, including 271 intra-residue, 116 sequential, 55 medium-range, and 40 long-range restraints. The distribution of these NOE and violations, provided by ARIA, is presented in Table I. In addition, 14 hydrogen bond restraints, derived from proton exchange, and 28 dihedral angle restraints, derived from the measurement of coupling constants, were included, as well as 15 distance restraints derived from the disulfide bridges. Altogether, the final experimental set corresponded to 12.3 constraints per residue on average. The calculation using the whole set of restraints and water solvent minimization led to a single family of 25 structures. Structural statistics are given in Table II. All the solutions have good nonbonded contacts and covalent

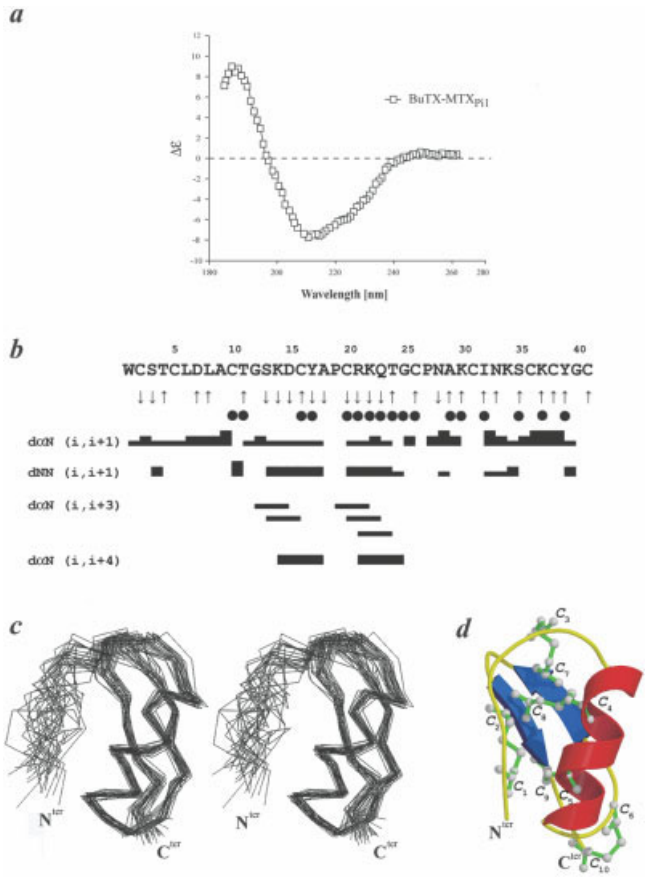

Fig. 4. Circular dichroism analysis and ^{1}H-NMR structure of BuTX-MTX$_{Pi1}$. **a:** Circular dichroism spectra of BuTX-MTX$_{Pi1}$ (□). **b:** Amino acid sequence of BuTX-MTX$_{Pi1}$ and sequential assignments. Collected sequential NOE's are classified into strong, medium, and weak NOE, and are indicated by thick, medium, and thin lines respectively. The up-arrows indicate $^{3}J_{HN\text{-}H\alpha}$ coupling constants ≥ 8 Hz and the down-arrows those that are ≤ 6 Hz. The nonexchanged amide protons are indicated. **c:** Stereo views of the 25 best molecular BuTX-MTX$_{Pi1}$ structures (only backbone atoms are displayed [Cα, HN, CO]) superimposed for best fit. N^{ter} and C^{ter} correspond to N- and C-terminal extremities. **d:** Molscript ribbon drawing of the average minimized BuTX-MTX$_{Pi1}$ structure. The helix, anti-parallel β-sheet, C$_{\alpha}$ backbone trace and disulfide bridges are shown in red, blue, yellow, and green, respectively. The ten half-cystine residues are numbered by order of appearance from the N- to the C-terminus of BuTX-MTX$_{Pi1}$.

TABLE I. NOE and Experimental Restraints Data

Conformational restraints	
NOE	482
Unambiguous restraints	464
Intraresidual, $\|i-j\|=0$	271
Sequential, $\|i-j\|=1$	116
Medium range, $\|i-j\|\leq 4$	55
Long range, $\|i-j\|\geq 5$	40
Ambiguous restraints[a]	18
Dihedral angles restraints	28
Hydrogen bonds	14
Restraint violations (number per structure)	
Distance restraints > 0.3 Å	0
Dihedral angle restraints > 5°	0

[a]Ambiguous distance restraints contain contribution from distances between all pairs of protons that are possible assignments of the NOE.

TABLE II. Structural Statistics of the 25 Best Structures of BuTX-MTX$_{Pi1}$

RMSD from standard geometry	
Bonds (Å)	0.0035 ± 0.0002
Angles (°)	0.5262 ± 0.0239
Impropers (°)	1.5402 ± 0.1940
Dihedral (°)	41.0870 ± 0.5031
RMSD from the experimental restraints	
NOE (Å)	0.0150 ± 0.0023
Constrained dihedrals (°)	0.4128 ± 0.1863
Energies (kcal/mol)	
Total	−1142.67 ± 43.93
Bonds	7.39 ± 0.66
Angles	45.38 ± 4.11
Impropers	26.40 ± 5.62
Dihedrals	195.08 ± 3.60
Van der Waals (repel)	−113.29 ± 9.02
Electrostatic	−1309.93 ± 42.90
NOE	5.89 ± 1.83
Constrained dihedrals	0.33 ± 0.24

Average RMSD (pairwise, Å)[a]

	Backbone (N, Cα, C)	All heavy atoms
Residues 1–41	1.71 ± 0.48	2.51 ± 0.51
Residues 9–40	0.80 ± 0.19	1.67 ± 0.29

[a]Calculated using MOLMOL.

geometry as shown by the low values of CNS energy terms and low RMSD values for bond lengths, valence, and improper dihedral angles. Correlation with the experimental data shows no NOE-derived distance violation greater than 0.3 Å. The analysis of the Ramachandran plot for the whole set of the 25 calculated structures reveals that 75.4% of the residues are in the most favored regions, 22.7% in the additional allowed regions, 1.9% in the generously allowed regions, and none in the disallowed regions (data not shown). The 3-D structure of BuTX-MTX$_{Pi1}$ can be described by the convergence of the 25 final structures. It displays the typical α/β scaffold consisting in an helix and a two stranded β-sheet stabilized by two disulfide-bridges (Cys^{16}-Cys^{36} and Cys^{20}-Cys^{38}). From this structured core emerges an extended region (residues 1 to 7) that contains the first disulfide bridge (Cys^{2}-Cys^{5}). Two disulfide bridges link the loop before the helix and the first β-strand (Cys^{10}-Cys^{31}) and the C-terminus with the loop between the helix and the first β-strand (Cys^{26}-Cys^{41}). Figure 4(c) shows a stereopair representation of the best-fit superimposition of the backbone traces of the 25 best structures and Figure 4(d) shows a MOLSCRIPT representation of the average structure. The RMSD calculated on the whole structure is 1.71 ± 0.48 Å for the backbone and 2.51 ± 0.51 Å for all heavy atoms. The RMSD values of region 1 to 6 is 1.14 ± 0.39 Å for the backbone and 2.46 ±

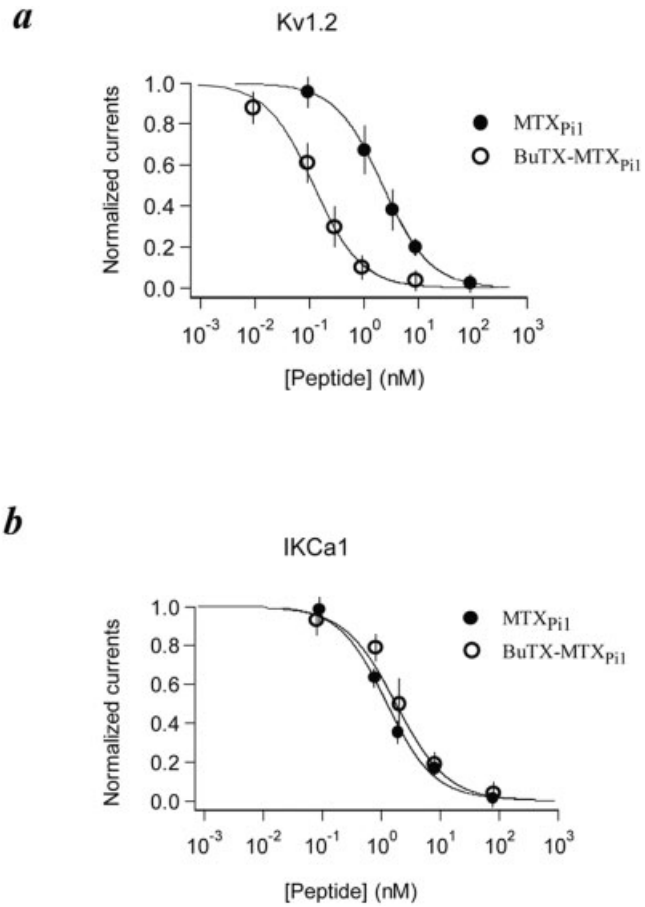

Fig. 5. Pharmacological activity of BuTX-MTX_{Pi1} and MTX_{Pi1}. **a:** Concentration-dependent inhibition curves of Kv1.2 currents by BuTX-MTX_{Pi1} (○) and MTX_{Pi1} (●). Fits of the data yield IC_{50} values of 0.13 ± 0.01 nM (BuTX-MTX_{Pi1}) and 2.8 ± 2.0 nM (MTX_{Pi1}) for Kv1.2. **b:** Concentration-dependent inhibition curves of IKCa1 currents by BuTX-MTX_{Pi1} (○) and MTX_{Pi1} (●). Fits of the data yield IC_{50} values of 2.2 ± 0.2 nM (BuTX-MTX_{Pi1}) and 0.9 ± 0.1 nM (MTX_{Pi1}) for IKCa1.

0.60 Å for all heavy atoms. These values fall to 0.80 ± 0.19 Å and 1.67 ± 0.29 Å, respectively, if region 9–40 is considered. This indicates an accurate structure for the MTX_{Pi1} part of the chimera. The region corresponding to the N-terminus of BuTX is less well-defined while possessing an extended structure. The larger RMSD values obtained for the whole structure are caused by the flexibility of the loop formed by residues 6–9.

Pharmacological Activity of BuTX-MTX_{Pi1}

In patch-clamp experiments, the effects of BuTX-MTX_{Pi1} and MTX_{Pi1} were compared on Kv1.2 potassium currents [Fig. 5(a)]. The concentration-dependent curves reveal that BuTX-MTX_{Pi1} and MTX_{Pi1} block Kv1.2 channels with IC_{50} values of 0.13 ± 0.01 nM and 2.8 ± 2.0 nM. It thus appears that swapping the N-terminal VS motif of MTX_{Pi1} by the N-terminal WCSTCLDLA motif of BuTX results in a 22-fold increase in blockage efficacy. We next compared the ability of both MTX_{Pi1} and BuTX-MTX_{Pi1} to block IKCa1 currents [Fig. 5(b)]. As shown in this figure, the IC_{50} value for IKCa1 current blockage by BuTX-MTX_{Pi1} (2.2 ± 0.2 nM) is not markedly different from that of MTX_{Pi1} (0.9 ± 0.1 nM). This was expected since the activities of BuTX and $BuTX_{\Delta 1-9}$ on IKCa1 channel are similar, indicating that the N-terminal region of BuTX does not contribute to its blocking efficacy on this channel type [Fig. 2(c)]. The increased activity of BuTX-MTX_{Pi1} on Kv1.2 suggests that at least some of the molecular contacts made with the channel by the N-terminal domain of BuTX may be conserved once this domain has been swapped into MTX_{Pi1}. We thus performed molecular docking simulations to check this point.

Docking Simulation of BuTX-MTX_{Pi1} onto the Kv1.2 Channel

First, a BLASTP request was performed against the whole Protein Data Bank to select the correct template that could be used to generate models of the S5-H5-S6 segment of the Kv1.2 channel. The primary structure of KvAP (Swiss-Prot # 1ORQ) showed the best E-value score for Kv1.2 (the use of KvAP as a premium template was confirmed by CLUSTALW, as indicated in the Experimental Procedures). The geometric quality of the generated models was assessed by the PROCHEK software (V 3.5.4); no amino acid was found to be in disallowed regions.

The 3-D structure of BuTX-MTX_{Pi1} was then used in docking simulations with the Kv1.2 channel. The binding of the chimera seems to be stabilized over the channel pore by sharing contacts with residues of both the pore entryway and the extracellular loop. BuTX-MTX_{Pi1} appears to be more stabilized than MTX_{Pi1} and BuTX onto the Kv1.2 channel, because of a greater number of close contacts (H-bonds and electrostatic interactions) [Fig. 6(a,b)]. It is stabilized over the pore region by several strong interactions (H-bonds) between, in particular, Thr^{11} and IQ^{357}, Asn^{33} and $IIAsp^{355}$, Lys^{34} and $IIVal^{381}$/$IIThr^{383}$, Lys^{37} and $IIGln^{357}$, Tyr^{39} and $IVGln^{357}$. It should be noted that Lys^{37} of BuTX-MTX_{Pi1} corresponds to Lys^{30} of MTX_{Pi1}, one residue that was shown to be pivotal for MTX bioactivity, including its recognition of the Kv1.2 channel.[6,38] Moreover, BuTX-MTX_{Pi1} possesses a number of contacts with Asp^{379} (Asn^{28} and Lys^{30} of the chimera with Asp^{379} of the channel Kv1.2 α-subunits IV and III, respectively), a residue critical for the binding of MTX onto Kv1.2 channel.[29] Interestingly, specific BuTX-MTX_{Pi1} residues, previously described for BuTX, are also in contact with the channel turret region (Trp^{1} with $IIIGln^{357}$, and Thr^{4} with $IVAsp^{355}$). This presumably results from a distinct orientation of this N-terminal region towards the channel. From these data, it appears that the greater affinity of the chimera would rely on a combination of molecular contacts related to both BuTX (mainly the stabilization with the channel turret) and MTX residues (mainly close contacts over the pore region).

For each best docking solution of BuTX, MTX_{Pi1}, or BuTX-MTX_{Pi1}/Kv1.2 channel complex, a docking energy was calculated according to the formula given in the Experimental Procedures. As shown in Figure 6(c), these

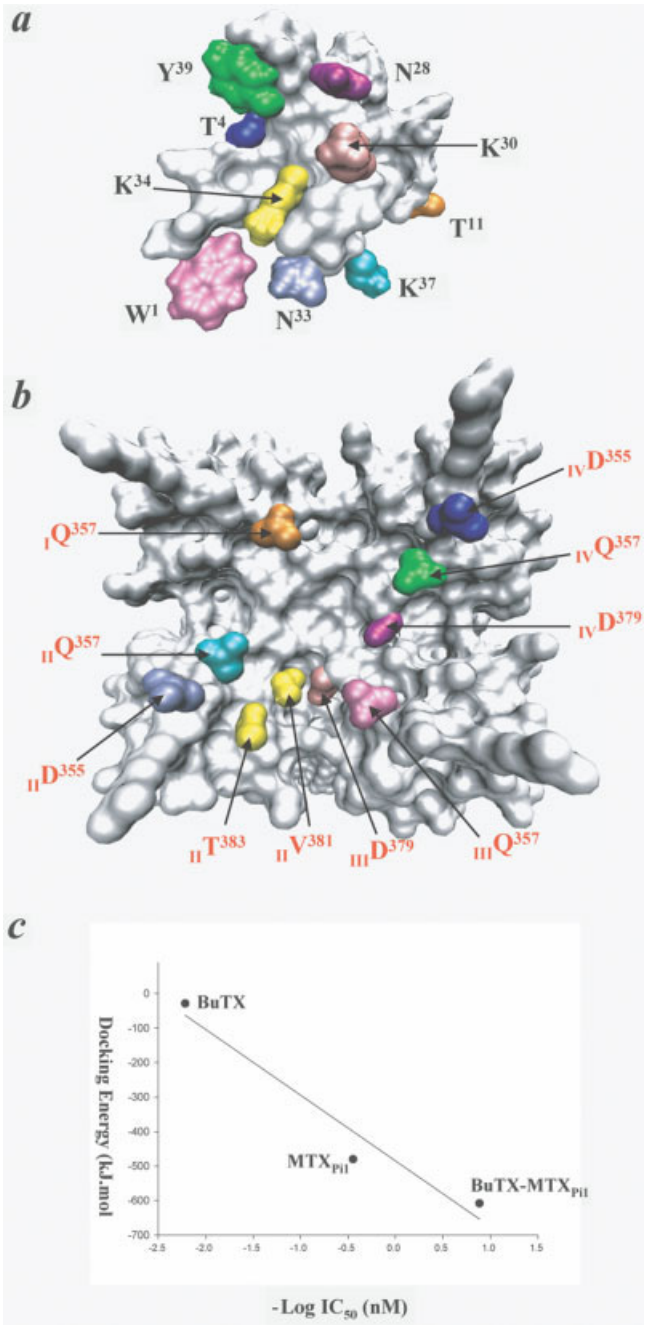

Fig. 6. Docking simulation of BuTX-MTX_{Pi1} onto Kv1.2 channel. **a:** Theoretical functional map of BuTX-MTX_{Pi1} highlighting amino acid residues that are key for the chimera interaction with Kv1.2 channel (colored residues). This map was generated by docking simulations. **b:** Molecular model of Kv1.2 detailing the major molecular contacts with BuTX-MTX_{Pi1}. Interacting residues from the Kv1.2 channel are shown in red. I to IV before channel residue numbering specifies one of the four α-subunits forming the functional Kv1.2 channel. The docking of BuTX-MTX_{Pi1} onto the Kv1.2 channel can be imagined by a 180° vertical rotation of BuTX-MTX_{Pi1}. Note that the magnification scales for BuTX-MTX_{Pi1} and Kv1.2 are different. **c:** Linear regression showing the correlation between docking energies and experimental IC_{50} values for BuTX, MTX_{Pi1} and BuTX-MTX_{Pi1} onto the Kv1.2 channel. The coefficient of correlation r^2 is 0.94.

values of energy could be well correlated with the experimental IC_{50} values for Kv1.2 channel blockage. The good correlation ($r^2 = 0.94$) suggests the existence of a linear relation between toxin/channel docking energies and experimental IC_{50} values.[6]

Concluding Remarks

Here, we have described the chemical synthesis of a five-disulfide-bridged chimera that is derived from the structures of two molecules (MTX_{Pi1}, a well-characterized peptide, and BuTX, a less well-defined toxin). The resulting chimera, BuTX-MTX_{Pi1}, was designed in order to examine the hypothesis that enriching a peptide with additional molecular contacts for a given channel type might result in an increase of peptide affinity for this channel. Our data indicate this approach has been successful. The transfer of the N-terminal domain of BuTX, exhibiting molecular contacts with Kv1.2, towards the N-terminal region of MTX_{Pi1} produces a chimera that is of greater affinity for Kv1.2. Molecular modeling indicates that this domain swapping could be also successful at a structural level since the molecular contacts, initially "functional" in BuTX, remained also "functional" in the context of the chimera. This positive outcome is based on a careful design of the chimera and the choice of an appropriate locus for domain swapping, which maintains the integrity of the MTX_{Pi1} secondary structures. The structural outcome of this approach is also of interest since the chimera still folds according to the canonical α/β scaffold in spite of the presence of an additional disulfide bridge in the molecule (five disulfide bridges). We conclude that such a selective "gain of function" strategy represents an interesting route to produce toxin analogues with novel properties.

ACKNOWLEDGMENTS

The authors wish to thank Drs. B. De Rougé, C. Devaux, and E. Doria for helpful discussions. This work was supported by funds from Inserm, the CNRS, and Cellpep SA.

REFERENCES

1. Kharrat R, Mansuelle P, Sampieri F, Crest M, Oughideni R, Van Rietschoten J, Martin-Eauclaire M-F, Rochat H, El Ayeb M. Maurotoxin, a four disulfide bridge toxin from Scorpio maurus venom: purification, structure and action on potassium channels. FEBS Lett 1997;406:284–290.
2. Kharrat R, Mabrouk K, Crest M, Darbon H, Oughideni R, Martin-Eauclaire MF, Jacquet G, El Ayeb M, Van Rietschoten J, Rochat H, Sabatier JM. Chemical synthesis and characterization of maurotoxin, a short scorpion toxin with four disulfide bridges that acts on K+ channels. Eur J Biochem 1996;242:491–498.
3. Fajloun Z, Ferrat G, Carlier E, Fathallah M, Lecomte C, Sandoz G, di Luccio E, Mabrouk K, Legros C, Darbon H, and others. Synthesis, 1H NMR structure, and activity of a three-disulfide-bridged maurotoxin analog designed to restore the consensus motif of scorpion toxins. J Biol Chem 2000;275:13605–13612.
4. Castle NA, London DO, Creech C, Fajloun Z, Stocker JW, Sabatier JM. Maurotoxin: a potent inhibitor of intermediate conductance Ca^{2+}-activated potassium channels. Mol Pharmacol 2003;63:409–418.
5. Fajloun Z, Mosbah A, Carlier E, Mansuelle P, Sandoz G, Fathallah M, di Luccio E, Devaux C, Rochat H, De Waard M, and others. Maurotoxin versus Pi1/HsTx1 scorpion toxins. Toward new in-

sights in the understanding of their distinct disulfide bridge patterns. J Biol Chem 2000;15:39394–39402.
6. M'Barek S, Lopez-Gonzalez I, Andreotti N, Di Luccio E, Visan V, Grissmer S, Judge S, El Ayeb M, Darbon H, Rochat H, and others. A maurotoxin with constrained standard disulfide bridging: innovative strategy of chemical synthesis, pharmacology, and docking on K^+ channels. J Biol Chem 2003;278:31095–31104.
7. di Luccio E, Azulay D, Regaya I, Fajloun Z, Sandoz G, Mansuelle P, Kharrat R, Fathallah M, Carrega L, Estéve, E, and others. Parameters affecting in vitro oxidation/folding of maurotoxin, a four-disulphide-bridged scorpion toxin. Biochem J 2001;358:681–692.
8. di Luccio E, Matavel A, Opi S, Regaya I, Sandoz G, M'Barek S, Carlier E, Estéve E, Carrega L, Fajloun Z, and others. Evolution of maurotoxin conformation and blocking efficacy towards Shaker B channels during the course of folding and oxidation in vitro. Biochem J 2002;361:409–416.
9. Regaya I, Beeton C, Ferrat G, Andreotti N, Darbon H, De Waard M, Sabatier JM. Evidence for domain-specific recognition of SK and Kv channels by MTX and HsTx1 scorpion toxins. J Biol Chem 2004;279:55690–55696.
10. Holaday SK, Martin BM, Fletcher PR, Krishna NR. NMR solution structure of butantoxin. Arch Biochem Biophys 2000;379:18–27.
11. Pimenta AM, Mansuelle P, Diniz CR, Martin-Eauclaire MF. Covalent structure and some pharmacological features of native and cleaved alpha-KTx12–1, a four disulfide-bridged toxin from *Tityus serrulatus* venom. J Peptide Sci 2003;9:132–140.
12. Grissmer S, Nguyen AN, Aiyar J, Hanson DC, Mather RJ, Gutman GA, Karmilowicz MJ, Auperin DD, Chandy KG. Pharmacological characterization of five cloned voltage-gated K^+ channels, types Kv1.1, 1.2, 1.3, 1.5, and 3.1, stably expressed in mammalian cell lines. Mol Pharmacol 1994;45:1227–1234.
13. Merrifield RB. Solid phase synthesis. Science 1986;232:341–347.
14. Hamill OP, Marty A, Neher E, Sakmann B, Sigworth FJ. Improved patch-clamp techniques for high-resolution current recording from cells and cell-free membrane patches. Pflugers Arch 1981;391:85–100.
15. Rauer H, Grissmer S. Evidence for an internal phenylalkylamine action on the voltage-gated potassium channel Kv1.3. Mol Pharmacol 1996;50:1625–1634.
16. Marion D, Ikura M, Tschudin R, Bax A. Rapid recording of 2D NMR spectra without phase cycling. Application to the study of hydrogen exchange in proteins. J Magn Res 1989;85:393–399.
17. Marion D, Wüthrich, K. Application of phase sensitive two-dimensional correlated spectroscopy (COSY) for measurements of 1H–1H spin-spin coupling constants in proteins. Biochem Biophys Res Commun 1983;113:967–974.
18. Piotto M, Saudek V, Sklenar V. Gradient-tailored excitation for single-quantum NMR spectroscopy of aqueous solutions. J Biomol NMR 1992;2:661–665.
19. Wüthrich, K, editor. NMR of proteins and nucleic acids. New-York: Wiley; 1986.
20. Eccles C, Guntert P, Billeter M, Wüthrich, K. Efficient analysis of protein 2D NMR spectra using the software package EASY. J Biomol NMR 1991;1:111–130.
21. Linge JP, Habeck M, Rieping W, Nilges M. ARIA: automated NOE assignment and NMR structure calculation. Bioinformatics 2003; 19:315–316.
22. Brunger AT, Adams PD, Clore GM, DeLano WL, Gros P, Grosse-Kunstleve RW, Jiang JS, Kuszewski J, Nilges M, Pannu NS, and others. Crystallography & NMR system: a new software suite for macromolecular structure determination. Acta Crystallogr D Biol Crystallogr 1998;54:905–921.
23. Roussel A, Cambillau C. Silicon Graphics Geometry Partner Directory. Mountain View, CA: Silicon Graphics; 1989. p 77–78.
24. Laskowski RA, Rullmannn JA, MacArthur MW, Kaptein R, Thornton JM. AQUA and PROCHECK-NMR: programs for checking the quality of protein structures solved by NMR. J Biomol NMR 1996;8:477–486.
25. Jiang Y, Lee A, Chen J, Ruta V, Cadene M, Chait BT, Mackinnon R. X-ray structure of a voltage-dependent K+ channel. Nature 2003;423:33–41.
26. Palma PN, Krippahl L, Wampler JE, Moura JJ. BiGGER: a new (soft) docking algorithm for predicting protein interactions. Proteins 2000;39:372–384.
27. Mouhat S, Jouirou B, Mosbah A, De Waard M, Sabatier JM. Diversity of folds in animal toxins acting on ion channels. Biochem J 2004;378:717–726.
28. Nicholls A, Sharp KA, Honig B. Protein folding and association: insights from the interfacial and thermodynamic properties of hydrocarbons. Proteins 1991;11:281–296.
29. Stocker U, van Gunsteren WF. Molecular dynamics simulation of hen egg white lysozyme: a test of the GROMOS96 force field against nuclear magnetic resonance data. Proteins 2000;40:145–153.
30. Wallace AC, Laskowski RA, Thornton JM. LIGPLOT: a program to generate schematic diagrams of protein-ligand interactions. Protein Eng 1995;8:127–134.
31. Carlier E, Fajloun Z, Mansuelle P, Fathallah M, Mosbah A, Oughideni R, Sandoz G, di Luccio E, Geib S, Regaya I, and others. Disulfide bridge reorganization induced by proline mutations in maurotoxin. FEBS Lett 2001;489:202–207.
32. Fajloun Z, Ferrat G, Carlier E, M'Barek S, Regaya I, Fathallah M, Rochat H, Darbon H, De Waard M, Sabatier JM. Synthesis, 3-D structure, and pharmacology of a reticulated chimeric peptide derived from maurotoxin and Tsk scorpion toxins. Biochem Biophys Res Comm 2002;291:640–648.
33. Rodriguez de la Vega RC, Possani LD. Current views on scorpion toxins specific for K^+-channels. Toxicon 2004;43:865–875.
34. Bontems F, Roumestand C, Gilquin B, Ménez A, Toma F. Refined structure of charybdotoxin: common motifs in scorpion toxins and insect defensins. Science 1991;254:1521–1523.
35. Blanc E, Sabatier JM, Kharrat R, Meunier S, El Ayeb M, Van Reitschoten J, Darbon H. Solution structure of maurotoxin, a scorpion toxin from Scorpio maurus, with high affinity for voltage-gated potassium channels. Proteins 1997;29:321–333.
36. Johnson WC. Circular dichroism and its empirical application to biopolymers. Methods Biochem Anal 1985;31:61–163.
37. Rogowski RS, Collins JH, O'Neill TJ, Gustafson TA, Werkman TR, Rogawski MA, Tenenholz TC, Weber DJ, Blaustein MP. Three new toxins from the scorpion Pandinus imperator selectively block certain voltage-gated K^+ channels. Mol Pharmacol 1996;50:1167–1177.
38. Fu W, Cui M, Briggs JM, Huang X, Xiong B, Zhang Y, Luo X, Shen J, Ji R, Jiang H, and others. Brownian dynamics simulations of the recognition of the scorpion toxin maurotoxin with the voltage-gated potassium ion channels. Biophys J 2002;83:2370–2385.